Endothelialization of chitosan porous conduits via immobilization of a recombinant fibronectin fragment ($rhFNIII_{7–10}$)

I.F. Amaral, I. Neiva, F. Ferreira da Silva, S.R. Sousa, A.M. Piloto, C.D.F. Lopes, M.A. Barbosa, C.J. Kirkpatrick[e], A.P. Pêgo

ABSTRACT

The present study aimed to develop a pre-endothelialized chitosan (CH) porous hollowed scaffold for application in spinal cord regenerative therapies. CH conduits with different degrees of acetylation (DA; 4% and 15%) were prepared, characterized (microstructure, porosity and water uptake) and functionalized with a recombinant fragment of human fibronectin ($rhFNIII_{7–10}$). Immobilized $rhFNIII_{7–10}$ was characterized in terms of amount (^{125}I-radiolabelling), exposure of cell-binding domains (immunofluorescence) and ability to mediate endothelial cell (EC) adhesion and cytoskeletal rearrangement. Functionalized conduits revealed a linear increase in immobilized $rhFNIII_{7–10}$ with $rhFNIII_{7–10}$ concentration, and, for the same concentration, higher amounts of $rhFNIII_{7–10}$ on DA 4% compared with DA 15%. Moreover, $rhFNIII_{7–10}$ concentrations as low as 5 and 20 $\mu g\ ml^{-1}$ in the coupling reaction were shown to provide DA 4% and 15% scaffolds, respectively, with levels of exposed cell-binding domains exceeding those observed on the control (DA 4% scaffolds incubated in a 20 $\mu g\ ml^{-1}$ human fibronectin solution). These grafting conditions proved to be effective in mediating EC adhesion/cytoskeletal organization on CH with DA 4% and 15%, without affecting the endothelial angiogenic potential. $rhFNIII_{7–10}$ grafting to CH could be a strategy of particular interest in tissue engineering applications requiring the use of endothelialized porous matrices with tunable degradation rates.

Keywords:
Three-dimensional scaffolds
Surface grafting
Protein radiolabelling
Protein conformation
Spinal cord injury

1. Introduction

Spinal cord injury (SCI) is a devastating condition, leading often to persistent loss of sensory, motor and autonomic function below the site of injury. Following SCI, neural and vascular structures are disrupted, and a series of complex events occur, including inflammation and disruption of the blood/spinal cord barrier, leading to progressive cell death, demyelination and enlargement of the damaged area culminating in the formation of a glial scar [1]. In preclinical studies, improved functional recovery after SCI has been achieved through the use of therapies focused on stem cell transplantation, delivery of neurotrophic factors, antagonism of neurite-outgrowth inhibitors, modulation of the inflammatory response, and use of bridging support matrices [2–4]. However, to achieve bridging axonal regeneration and full functional recovery, combinations of complementary and synergistic therapeutic approaches integrating guidance matrices, cells and localized delivery of therapeutic molecules are likely to be required [3,4].

The use of single and multi-channelled nerve guidance tubes to bridge the cystic cavity formed following SCI contributes in different ways to the establishment of a more permissible microenvironment for axonal regeneration. Besides providing mechanical support for the lesion area and protecting it from the infiltration of inflammatory cells, they concentrate neurite-growth-promoting factors released from the severed nerve stumps, while also guiding axonal growth through intra luminal architecture [4]. Moreover, hydrogels containing cell suspensions and/or signalling molecules may be easily incorporated in their inner lumen [5,6]. These internal hydrogel matrices allow homogeneous cell distribution and provide physical support for axonal growth, apart from helping to sequester cell-secreted growth factors and preventing channel collapse [4].

The present study aimed to develop a pre-endothelialized chitosan (CH) porous hollowed scaffold for application in spinal cord

regenerative therapies. CH biodegradability and cytocompatibility with neural cells [7] associated with its versatility to be processed into flexible tubular and porous structures make it interesting for the design of guidance matrices. CH-based nerve guidance matrices have been successfully explored for peripheral nerve regeneration [8] and, more recently, for application in the spinal cord, in combination with cell transplantation therapies [9–11]. CH degradation in vivo is thought to be mediated predominantly by lysozyme [12], an enzyme normally present in the cerebrospinal fluid at low concentrations, though upregulated after SCI [13,14]. The susceptibility of CH to lysozyme-mediated degradation is directly influenced by its degree of acetylation (DA) [15], with higher DAs leading to faster degradation rates in vivo [16]. CH degradation can, therefore, be tuned by varying the DA. The effect of DA on CH degradation profile in the spinal cord was investigated recently in non-immunosuppressed rats, using non-porous CH matrices with DA 15% and 22% [17]. Even though both matrices were considered suitable for long-term spinal cord applications, DA 15% implants were shown to elicit a weaker inflammatory response. However, with respect to CH porous structures, the range of DA adequate for this application is still an issue to be addressed.

Endothelialization of guidance matrices is a novel approach in the context of SCI therapies. Apart from secreting trophic factors [18] that may contribute per se to create a more favourable environment for regeneration, endothelial cells (ECs) are expected to contribute to angiogenesis in vivo and, hopefully, to the establishment of a functional microvascular network upon implantation. Both effects will be important to enhance the survival of co-transplanted cells, such as mesenchymal stem or neural progenitor cells, which in turn may contribute to vessel stabilization [19].

Previous work showed that colonization of CH scaffolds by EC could be achieved by physically adsorbing human fibronectin (hFN) to CH [20], the most frequent approach to promoting EC adhesion to polymeric biomaterials [21]. Nevertheless, the effectiveness of hFN physiadsorption in mediating EC adhesion to CH was found to be strongly dependent on the DA. More precisely, hFN physiadsorption was only effective in promoting cell adhesion to CH with a low DA (4%) and not to CH with DA 15%, which, despite its poorer cell adhesive properties may also be an interesting polymer for the application in view, as it presents a faster degradation rate. Besides developing CH porous tubular scaffolds for use in SCI therapies, this work explored a strategy to promote EC adhesion to CH with different DAs. This was pursued by covalently binding to CH scaffolds, a recombinant fragment of hFN, rhFN $III_{7–10}$, which includes the arginine–glycine–aspartic acid (RGD) integrin-binding motif of the 10th type III repeat and the pro- line–histidine–serine–arginine–asparagine (PHSRN) synergy site domain on the 9th type III repeat [22].

2. Materials and methods

2.1. CH purification and characterization

Squid pen CH (Batch No. 171204; DA 1.5%) was supplied by France Chitine and, subsequently, purified by filtration of CH acidic solution, followed by alkali precipitation. The purified CH was characterized in terms of DA and average molecular weight by Fourier transform infrared spectroscopy (FTIR) and size exclusion chromatography, respectively, as previously described [20]. A DA of $3.55 \pm 0.32\%$, with weight-average molecular weight (M_w) $5.0 \pm 0.2 \times 10^5$ and polydispersity index (PDI) 1.8 ± 0.1 were found. CH with DA rv15% was prepared by *N*-acetylation of the purified CH according to Vachoud et al. [23]. Subsequent analysis revealed a DA of 15.35 ± 1.26, M_w $4.3 \pm 0.1 \times 10^5$ and a PDI of 2.2 ± 0.1. Endotoxin levels were measured in water extracts using the Limulus Amebocyte Lysate Assay (QCL-1000, Cambrex). The two polymers revealed endotoxin levels <0.1 EU ml^{-1}, respecting the US Department of Health and Human Services guidelines for implantable devices [24].

2.2. Preparation and characterization of CH cylindrical hollowed porous scaffolds

CH porous conduits with a porous luminal surface were prepared from degassed 2% w/v CH solutions in 0.2 M acetic acid solution by thermally induced phase separation (−80 °C) and subsequent sublimation of ice crystals. Poly(vinyl chloride) (PVC) tubes (25 mm in length; $Ø_{ext} = 6.08$ mm; $Ø_{int} = 3.85$ mm) with a plastic wire (Ø = 1.83 mm) inserted in the inner part were used as moulds. Following lyophilization (−86 °C; 0.2 mbar), the external PVC mould was removed, and the resultant scaffolds sequentially immersed in serially diluted ethanol solutions and finally Milli-Q ultrapure water (Millipore), to eliminate acid. The internal wire was then removed, and the scaffolds lyophilized once again. The resultant porous conduits were cut into sections 4 mm long and characterized in terms of microstructure, porosity and water uptake. For microstructure analysis, the scaffolds were trimmed in liquid nitrogen into transversal and longitudinal cross sections, lyophilized and, finally, sputter-coated with gold before being examined by scanning electron microscopy (SEM). The average pore diameter and diameter of interconnecting pores were determined as previously described [20], analyzing 20 SEM images corresponding to transversal cross sections of at least three different samples. Porosity was assessed using the liquid displacement method, using absolute ethanol as the displacement liquid [25]. Prior to the analysis, samples were dried in a vacuum oven at 30 °C for 24 h and longitudinally sectioned. For each measurement, two scaffolds (9–12 mg) were used. For water uptake measurements, samples were dried, longitudinally sectioned, and then immersed in ultrapure water for 24 h at room temperature (RT). Prior to being used in the subsequent assays, the scaffolds were sterilized in 70% ethanol v/v and equilibrated in sterile phosphate-buffered saline (PBS).

2.3. Expression and purification of $rhFNIII_{7–10}$

The prokaryotic expression vector pET-15b with an insert coding for $rhFNIII_{7–10}$ (pET-15b–$rhFNIII_{7–10}$) was kindly provided by Dr. Harold P. Erickson (Duke University Medical Center). $rhFNIII_{7–10}$ was expressed in BL21(DE3) *Escherichia coli* transformed with the pET-15b–$rhFNIII_{7–10}$ plasmid, as described by Aukhil et al. [26]. Sodium dodecyl sulphate-polyacrylamide gel electrophoresis (SDS-PAGE) was used to check the presence of $rhFNIII_{7–10}$ in the soluble extract of bacterial lysates. $rhFNIII_{7–10}$ was purified by affinity chromatography (1 ml Bio-Scale Mini IMAC cartridge charged with Ni^{2+}; Bio-Rad) followed by buffer exchange to 20 mM Tris–HCl, pH 7.4 and ion exchange chromatography (1 ml HiTrap Q HP column, GE Healthcare) [27]. Following elution with a 0–500 mM NaCl gradient over 20 column volumes, purified $rhFNIII_{7–10}$ was dialyzed against 20 mM Tris–HCl pH 7.9 and its purity analysed by SDS-PAGE under reducing conditions. The purity of each fraction was determined by densitometry analysis, while the molecular weight was interpolated from a standard curve obtained by plotting the $\log_{10}$ of the molecular weight of the standard proteins vs. their relative mobility [28]. Purified $rhFNIII_{7–10}$ was characterized in terms of protein concentration (DC Protein Assay, Bio-Rad), flash frozen and finally stored at −80 °C. Before use, the protein aliquots were rapidly thawed, spun down and the concentration determined.

2.4. Immobilization of $rhFNIII_{7–10}$

Immobilization of $rhFNIII_{7–10}$ was performed using carbodiimide chemistry and 0.1 M 2-morpholinoethanesulfonic acid (MES)

buffer (pH 6.5). CH scaffolds were equilibrated in 0.1 M MES for 1 h under reduced pressure and then transferred to rhFNIII$_{7–10}$ solutions in 0.1 M MES with concentrations ranging from 2.5 to 80 μg ml^{-1}. After 15 min, *N,N*-(3-dimethylaminopropyl)-*N*-ethyl carbodiimide (EDC) and *N*-hydroxysuccinimide (NHS), previously dissolved in 0.1 M MES were added. EDC was added at 1 mol mol^{-1} of carboxilate moieties present in rhFNIII$_{7–10}$, and NHS was added at a molar ratio of 1:2 to EDC. Grafting was carried for 15 h at 37 °C in a thermostat-regulated orbital shaker (250 rpm), using 60 μl of rhFNIII$_{7–10}$ solution/scaffold. At the end of this period and to remove rhFNIII$_{7–10}$ electrostatically bound to the CH amine groups positively charged at pH 6.5 [29], scaffolds were incubated in PBS with pH 8.5 for 1 h. Finally, the samples were rinsed and squeezed (3x) in PBS. Physiadsorption of rhFNIII$_{7–10}$ was performed in parallel for comparison purposes, incubating the scaffolds in rhFNIII$_{7–10}$ solutions (2.5 to 80 μg ml^{-1}) in PBS for 15 h (37 °C; 250 rpm). CH scaffolds (DA 4%) incubated for 15 h in a 20 μg ml^{-1} hFN (Sigma) solution in PBS were used as controls.

2.5. Characterization of CH porous conduits grafted with rhFNIII$_{7–10}$

2.5.1. FTIR with attenuated total reflectance

The IR spectra were obtained with an FT-IR system 2000 (Perkin-Elmer) using the SplitPea™ accessory (Harrick Scientific) after accumulation of 200 interferograms at a 4 cm^{-1} spectral resolution. Prior to analysis, the scaffolds were dried at 60 °C in a vacuum oven for 12 h. All spectra were corrected for the attenuated total reflectance (ATR) characteristic progressive increase in the absorbance at lower wave numbers, using the equipment software.

2.5.2. ^{125}I-radiolabelling

The amount of rhFNIII$_{7–10}$ incorporated into CH was quantified using ^{125}I-rhFNIII$_{7–10}$ as a tracer molecule. rhFNIII$_{7–10}$ was labelled as previously described [30]. Fractions with yield of ^{125}I-labelling $\geq$98.8% were used. The labelled fragment was stored at −20 °C and used within 2 days. Prior to the grafting reaction, CH scaffolds were individually weighted, sterilized and hydrated as described above, and equilibrated overnight in degassed PBS with 0.01 M NaI, to prevent adsorption of free ^{125}I ions present in trace amounts in ^{125}I-rhFNIII$_{7–10}$. To assess whether preferential grafting of ^{125}I-labelled rhFNIII$_{7–10}$ or unlabelled rhFNIII$_{7–10}$ occurred, a series of control experiments were initially performed, varying the ratio of labelled to unlabelled rhFNIII$_{7–10}$. In all the subsequent grafting reactions, labelled solutions with a final activity of $\approx 4 \times 10^6$ cpm ml^{-1} were used. Functionalized samples were processed straight away for gamma activity counting or further incubated in 200 μl of the serum-containing medium used in cell culture assays for 24 h, to assess the amount of immobilized rhFNIII$_{7–10}$ retained in the presence of serum proteins. Prior to gamma activity counting, all samples were sequentially rinsed and squeezed in PBS (8x), immersed in PBS for 15 h at RT, and rinsed again in PBS (3x) to remove unbound rhFNIII$_{7–10}$. Fibronectin adsorption to CH was determined as previously described, using ^{125}I-hFN [20].

2.5.3. Exposure of cell-binding domains

The distribution and bioactivity of immobilized rhFNIII$_{7–10}$ was assessed by immunofluorescent staining of cell-binding domains. Three scaffolds per condition were flash frozen in liquid nitrogen and cryosectioned to yield transversal sections 100 μm thick. Samples were incubated with 1% w/v heat-denatured bovine serum (BSA) in PBS and then for 1 h with mouse monoclonal HFN 7.1 (Developmental Studies Hybridoma Bank) diluted to 1:1000. Detection was achieved with Alexafluor 568-conjugated anti-mouse IgG (Molecular Probes) diluted at 5 μg ml^{-1}. After being rinsed, samples were mounted with Fluoromount (Sigma) for confocal laser scanning microscopy (CLSM) imaging or transferred to the wells of 24-well tissue culture polystyrene plates, for quantitative analysis of fluorescence intensity (FI). The FI of each cryosection was read (k_{Ex} 578 nm; k_{Em} 603 nm) using a BioTek® Synergy™ MX plate reader with the optics position set to bottom. The FI values were determined by subtracting the FI value of samples incubated in 0.1 M MES without rhFNIII$_{7–10}$.

2.6. EC behaviour in porous conduits grafted with rhFNIII$_{7–10}$

2.6.1. Cell culture

A cell line of human pulmonary microvascular endothelial cells (HPMEC-ST1.6R cell line) displaying most of the major constitutively expressed and inducible endothelial phenotypic markers was used [31]. Cells were cultured in complete culture media (CCM) containing 20% (v/v) fetal bovine serum, as previously described [20].

2.6.2. Cell seeding

For cell adhesion and cytoskeleton organization studies, longitudinally sectioned porous conduits (hemi sections) were used. Cell seeding was performed by adding 9 μl of a cell suspension (3×10^6 cells ml^{-1} in CCM) to the luminal surface of the scaffolds. After a 3 h incubation period at 37 °C, the scaffolds were transferred to the wells of 48-well suspension culture plates (Cellstar®, Greiner Bio-one) and 500 μl of CCM were added. For the in vitro angiogenesis studies, EC were seeded in the lumen of the tubular scaffolds, using a two-step process. Initially, 2×10 μl of a cell suspension (3×10^6 cells ml^{-1} in CCM) were transferred to the lumen of the internal channel. After 3 h incubation at 37 °C, the scaffolds were rotated manually 180°, and the cell seeding procedure repeated, to ensure the homogeneous cell seeding of the luminal surface. Following a second incubation period of 3 h at 37 °C, the scaffolds were transferred to the wells of 48-well suspension culture plates, and 1 ml of CCM was added. The cell constructs were cultured for periods of up to 5 days, the medium being refreshed every other day.

2.6.3. Cell adhesion

Cell adhesion was inferred from cell metabolic activity, determined as described previously [20], 24 h after cell seeding using a resazurin-based assay. Fluorescence was measured (k_{Ex} 530 nm; k_{Em} 590 nm), and the fluorescence value corresponding to unseeded scaffolds subtracted. The cell number was extrapolated from a standard curve, where fluorescence was plotted against a known number of HPMECs seeded in parallel on hFN-coated wells and further incubated for 2 h to allow for cell adhesion.

2.6.4. Cytoskeletal organization

Cytoskeletal organization was assessed 24 h after cell seeding by F-actin/DNA fluorescent labelling, as described previously [32].

2.6.5. Angiogenic potential

The angiogenic potential of HPMEC-ST1.6R cells seeded on rhFNIII$_{7–10}$-grafted CH scaffolds was investigated after 5 days of cell culture by adding a fibrin gel to the EC-colonized scaffolds and culturing these in the presence of angiogenic stimuli. For this purpose, a fibrin gel was prepared by polymerization of fibrinogen in the presence of thrombin and $CaCl_2$ (final concentration in the polymerizing solution: 6 mg ml^{-1} plasminogen-free human fibrinogen; 2 NIH U ml^{-1} thrombin; 2.5 mM $CaCl_2$, all Sigma). The polymerizing fibrin gel (20 μl) was injected into the inner lumen of the porous conduits and the cell–matrix constructs incubated at 37 °C for 30 min to allow gel polymerization. At the end of this period, 1 ml

of CCM supplemented with 25 ng ml^{-1} of VEGF (Milllipore), 10 ng ml^{-1} of bFGF (Prepotech) and 5 μg ml^{-1} aprotinin (Sigma) was added to each EC-colonized scaffold, and the cells were cultured for an additional period of 48 h. To assess EC sprouting into the fibrin gel, samples were fixed in 3.7% PFA, embedded in gelatin, frozen in liquid nitrogen, cryosectioned at 100 μm thickness, and further processed for hematoxylin and eosin (H&E) staining. For live imaging of EC sprouting under CLSM, EC-colonized longitudinal hemisections of the porous scaffolds were embedded in the fibrin gel, and cultured as described above. After 48 h of cell culture, the cell–matrix constructs were incubated with calcein AM (4 μM; 37 °C; 30 min) and further with propidium iodide (6 μM; 37 °C; 10 min), for detection of viable and non-viable cells, respectively.

2.7. Statistical analysis

Reported values are the mean ± standard deviation. Sample distribution was tested for normality using the Kolmogorov–Smirnov test, and data subsequently analysed using the unpaired *t*-test. A 95% confidence level was considered statistically significant. Calculations were performed using IBM® SPSS® Statistics (version 19).

3. Results

3.1. Characterization of CH porous scaffolds

The moulding system described yielded porous conduits with reproducible size and structure, with inner and outer diameters of 1.8 and 3.6 mm, respectively. SEM analysis revealed outer and luminal surfaces of the conduits with open porosity and no evidence of skin formation (Fig. 1). At higher magnification, cross sections showed a highly porous and interconnected homogeneous microstructure, as well as the presence of round orifices in the thin polymeric walls delimiting the pores, corresponding to interconnecting pores (Fig. 1b and e). Subsequent image analysis of transversal cross sections further revealed values of pore diameter in the range 45–78 μm, and higher average pore diameter for DA 15% ($p < 0.001$, Table 1). In terms of interconnective pores, similar values of average diameter were found for the two types of scaffolds, namely in the range 22–24 μm (Table 1). In agreement with SEM results, porosity analysis revealed high values of porosity for both the DAs investigated (98.3%). Following immersion in water for 24 h, the lyophilized scaffolds absorbed more than 3400% of their initial weight, showing no apparent change in microstructure, as demonstrated by subsequent CLSM imaging of the hydrated samples (Fig. S1). As higher water uptake values were found for DA 15% compared with DA 4% ($p = 0.001$), water uptake measurements were also performed in CH films prepared from the same polymers (1% w/v in 0.2 M CH_3COOH). Results also revealed higher water uptake levels for DA 15% (233 ± 7%) compared with DA 4% (196 ± 6%).

3.2. rhFNIII$_{7–10}$ expression and purification

Elution of purified rhFNIII$_{7–10}$ was observed when an ionic strength of about 20 mS (rv200 mM NaCl) was used. Subsequent analysis of coomassie blue-stained SDS-PAGE gel of the eluted chromatography fractions (Fig. S2) of the purified fragment revealed a purity ranging from 96.1% to 97.3% and a molecular weight of 43.85 kDa, which is close to the molecular weight calculated from the amino acid sequence of this fragment (41.66 kDa) [27].

3.3. EC behaviour on CH porous conduits physiadsorbed with rhFNIII$_{7–10}$

To enable EC adhesion to CH, physiadsorption of rhFNIII$_{7–10}$ was initially explored. For this purpose, HPMEC-ST1.6R cells were seeded on CH porous conduits previously incubated with rhFNIII$_{7–10}$ (2.5–80 μg ml^{-1}), and the cytoskeleton of adhered cells investigated after 24 h of cell culture. Results showed that, in the case of DA 4%, rhFNIII$_{7–10}$ concentrations P20 μg ml^{-1} of rhFNIII$_{7–10}$ were as effective as hFN (20 μg ml^{-1}) in allowing EC cytoskeletal organization and scaffold colonization (Fig. 2a, c and

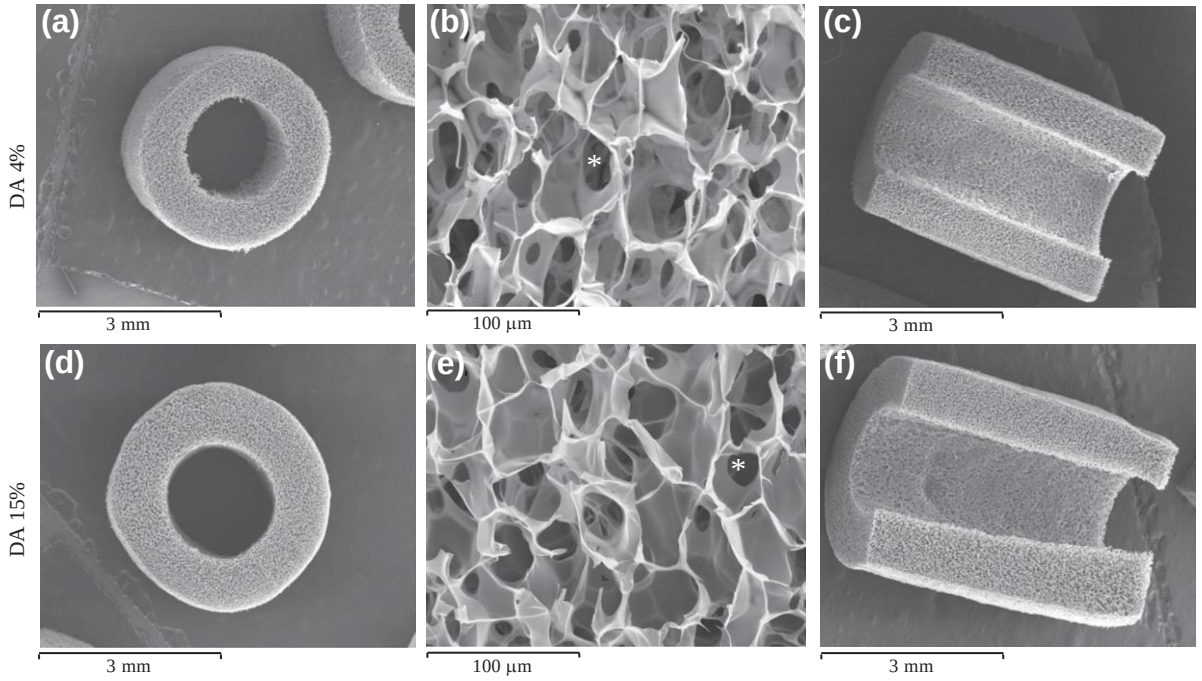

Fig. 1. SEM micrographs of dehydrated CH cylindrical hollowed porous scaffolds (DA 4% and 15%). Transversal (a, b, d, e) and longitudinal cross-sections (c and f) are shown. (b and e) depicts high magnification SEM micrographs, showing the presence of interconnecting pores (*) in the thin polymeric walls.

Table 1
Characterization of CH cylindrical hollowed porous scaffolds in terms of average pore diameter (mean ± SD; $n = 70$), average diameter of interconnecting pores (mean ± SD; $n = 70$), porosity (mean ± SD; $n = 3$), and water uptake (mean ± SD; $n = 5$).

DA (%)	Average pore diameter (μm)	Average diameter of interconnecting pores (μm)	Porosity (%)	Water uptake (%)
4	55.57 ± 10.41*	22.19 ± 8.15	98.3 ± 0.0	3449.4 ± 83.4*
15	64.07 ± 13.71	23.94 ± 8.34	98.3 ± 0.0	3752.4 ± 115.1

* p 6 0.001 vs. DA 15%.

e). However, in the case of DA 15%, the simple adsorption of rhFNIII$_{7–10}$ to the scaffolds was not sufficient to permit EC adhesion and cytoskeletal organization on CH, regardless of the rhFNIII$_{7–10}$ concentration used (Fig. 2d). In fact, most of the few ECs that remained attached to the scaffolds displayed a round-shaped morphology with faint F-actin staining, behaving similarly to ECs seeded on CH porous conduits merely incubated in CCM (Fig. S3). Only in the case of incubation of DA 15% scaffolds with 80 μg ml^{-1} of rhFNIII$_{7–10}$ was a modest improvement in EC adhesion and spreading observed (Fig. 2f), in the range of that provided by passively adsorbed hFN (Fig. 2b).

To provide an insight into the marked differences observed between the two DAs in terms of EC response to physiadsorbed rhFNIII$_{7–10}$, protein adsorption studies were performed. Radiolabelling assays using a range of ^{125}I-labelled rhFNIII$_{7–10}$ solutions (0.5–80 μg ml^{-1}) showed a linear increase in the adsorbed rhFNIII$_{7–10}$ with increasing rhFNIII$_{7–10}$ concentration ($R^2 = 0.9932$) and, for the same concentration (20 μg ml^{-1}), threefold lower amounts of adsorbed rhFNIII$_{7–10}$ on DA 15% compared with DA 4% (Fig. S4a and b). In line with these results, for the same rhFNIII$_{7–10}$ input concentration, lower numbers of exposed cell-binding domains were found on DA 15% scaffolds compared with DA 4% ($p < 0.001$; Fig. S5).

3.4. Immobilization of rhFNIII$_{7–10}$ onto CH porous conduits

As an alternative strategy to protein physiadsorption, the covalent binding of rhFNIII$_{7–10}$ to CH scaffold surface was addressed. To evaluate the effectiveness of EDC/NHS mediated amidation, CH scaffolds (DA 4%) were functionalized with rhFNIII$_{7–10}$ (80 μg ml^{-1}) in the absence or presence of EDC/NHS, and immobilized rhFNIII$_{7–10}$ detected by immunofluorescent labelling of FN cell-binding domains. Results revealed 12-fold higher FI levels following incubation in the presence of EDC/NHS compared with 0.1 M MES alone (Fig. S6).

3.4.1. ATR-FTIR spectroscopy

ATR-FTIR analysis was performed to study the nature of the coupling reaction. The ATR-FTIR spectra of functionalized CH scaffolds, as well as of the unmodified scaffolds, are presented in Fig. 3. The covalent binding of rhFNIII$_{7–10}$ to CH primary amines is supported by the decrease in the peak at 1585 cm^{-1} assigned to the N–H deformation in amines [33]. The decrease in the peaks at 1070 and 1032 cm^{-1} (C–O stretching and C–N stretching in >CH–NH_2 [33–35]) further confirms the grafting of rhFNIII$_{7–10}$ at the expense of CH primary amines. Spectrum analysis also revealed an increase in the Amide I peak (C@O stretching in primary amides)

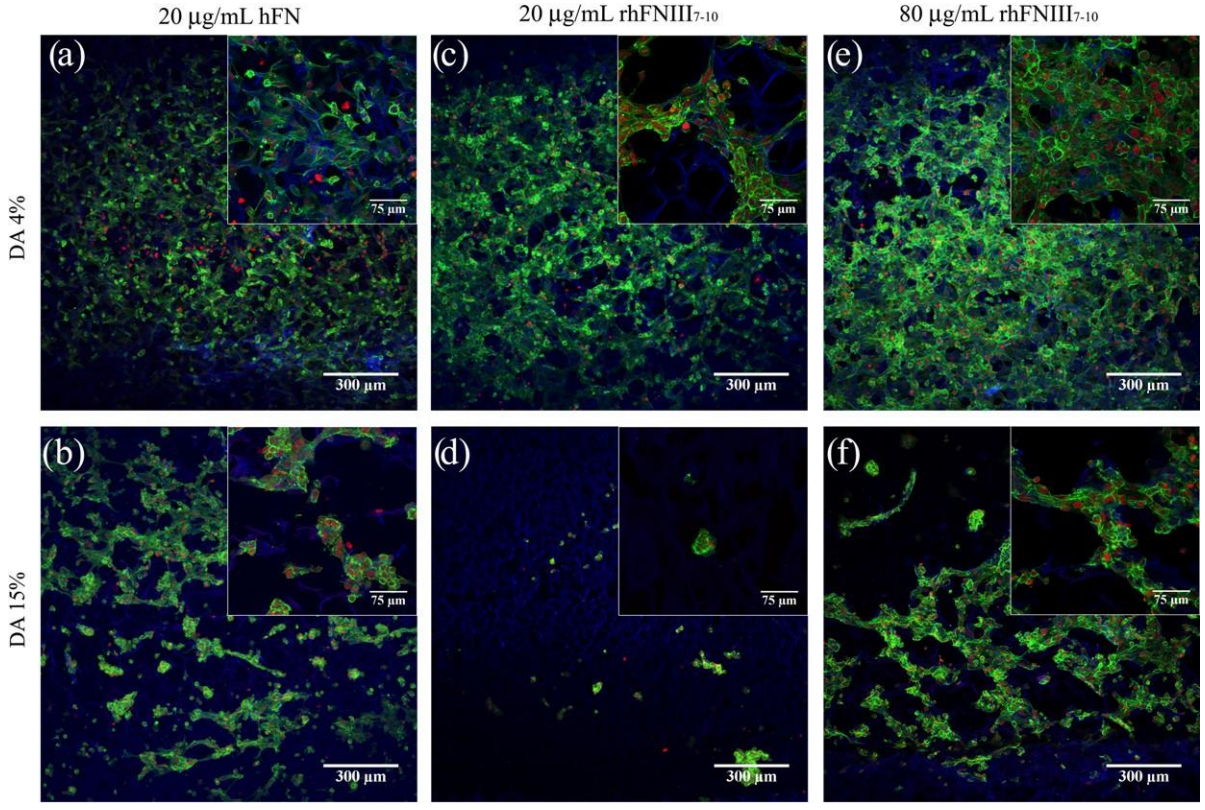

Fig. 2. Fluorescent labelling of F-actin (green) and DNA (red) of HPMEC-ST1. 6R cells cultured on CH porous conduits (DA 4% and 15%) previously incubated in a 20 μg ml^{-1} hFN solution (a and b) or in rhFNIII$_{7–10}$ solutions with concentrations of 20 (c and d) and 80 μg ml^{-1} (e and f). Images obtained by CLSM, 24 h after cell seeding. The polymeric structure is shown in blue due to CH autofluorescence upon excitation by the 405 nm laser.

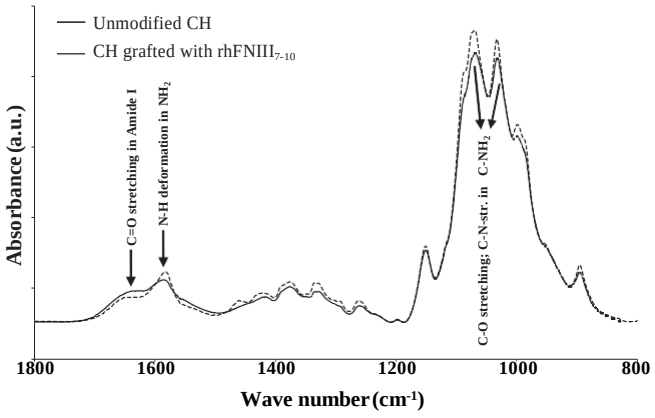

Fig. 3. ATR–FTIR spectra (1800–800 cm^{-1}) of CH porous conduits grafted with $rhFNIII_{7–10}$ (80 $\mu g\ ml^{-1}$; solid line) and unmodified CH porous conduits (dotted line). Spectra shown correspond to CH porous conduits with DA 4%.

at 1648 cm^{-1}, possibly due to the contribution of amide bonds from $rhFNIII_{7–10}$ to the amide I vibration. Moreover, the increase in Amide I peak intensity is also in accordance with the establishment of amide linkages between carboxylate moieties of $rhFNIII_{7–10}$ and CH amine groups.

3.4.2. Radioiodination assays

First, the effect of ^{125}I-labelled $rhFNIII_{7–10}$ on the grafting of $rhFNIII_{7–10}$ to CH was assessed. As no correlation between the ratio ^{125}I-$rhFNIII_{7–10}$/$rhFNIII_{7–10}$ used and the amount of immobilized $rhFNIII_{7–10}$ was found, ^{125}I-labelled $rhFNIII_{7–10}$ was used as a tracer to quantify $rhFNIII_{7–10}$ grafting to CH (Fig. S7). The results showed a linear increase of immobilized $rhFNIII_{7–10}$ amounts with increasing $rhFNIII_{7–10}$ concentration ($R^2 = 0.9914$), within the range of concentrations tested (Fig. 4a). Moreover, when the amounts of immobilized $rhFNIII_{7–10}$ are compared with those of passively adsorbed hFN, for the same input protein concentration (20 $\mu g\ ml^{-1}$), covalent binding was found to provide CH with higher amounts of protein (1.6- and 3.4-fold higher for DA 4% and 15%, respectively). Nevertheless, the DA was found to influence the levels of immobilized $rhFNIII_{7–10}$ on CH, DA 15% scaffolds revealing 2.5-fold lower amounts of $rhFNIII_{7–10}$ compared with DA 4% (Fig. 4b). Following subsequent incubation of the functionalized scaffolds in serum-containing medium for 24 h, partial elution of immobilized $rhFNIII_{7–10}$ occurred. Nevertheless, as expected, immobilized $rhFNIII_{7–10}$ showed higher retention in the presence of competitive proteins than physiadsorbed hFN, in the case of both DA 4% and DA 15% scaffolds (1.5- and 1.7-fold higher, respectively).

3.4.3. Exposure of cell-binding domains

The distribution and conformation of $rhFNIII_{7–10}$ upon grafting to CH were examined by immunofluorescent staining of cell-binding domains on cryosections (Fig. 5). For this purpose, the monoclonal HFN7.1 antibody that binds to the major cell-binding domain of hFN between the ninth and tenth type III repeat was used. This antibody has proved to be an effective probe for measuring FN functionality following adsorption onto different substrates, namely in terms of exposure of integrin binding sites [36]. Covalent binding of $rhFNIII_{7–10}$ resulted in a homogeneous distribution of $rhFNIII_{7–10}$ with exposure of cell-binding domains, as shown by CLSM (Fig. 5a). Subsequent fluorimetry analysis revealed an increase in FI levels with increasing $rhFNIII_{7–10}$ concentration and, in the case of DA 4%, a saturation plateau reached at 20 $\mu g\ ml^{-1}$ (Fig. 5b). In line with radioiodination results, DA 4% scaffolds showed significantly higher FI levels than DA 15%, regardless of the $rhFNIII_{7–10}$ concentration used, except for the highest concentration tested (80 $\mu g\ ml^{-1}$). Moreover, while for DA 4%, $rhFNIII_{7–10}$ concentrations as low as 5 $\mu g\ ml^{-1}$ were sufficient to provide CH conduits with levels of exposed cell-binding domains exceeding those provided by passively adsorbed hFN (20 $\mu g\ ml^{-1}$, control), for DA 15%, similar levels were only attained using 20 $\mu g\ ml^{-1}$ of $rhFNIII_{7–10}$.

3.5. EC behaviour in porous conduits grafted with $rhFNIII_{7–10}$

The ability of immobilized $rhFNIII_{7–10}$ to mediate EC adhesion to CH was subsequently investigated, and compared with that of passively adsorbed hFN. Immobilized $rhFNIII_{7–10}$ was shown to be as effective as passively adsorbed hFN (20 $\mu g\ ml^{-1}$, control) in promoting EC adhesion to DA 4%, for $rhFNIII_{7–10}$ concentrations as low as 5 $\mu g\ ml^{-1}$ (Fig. 6a). Most importantly, immobilized $rhFNIII_{7–10}$ allowed the attainment of similar cell numbers on DA

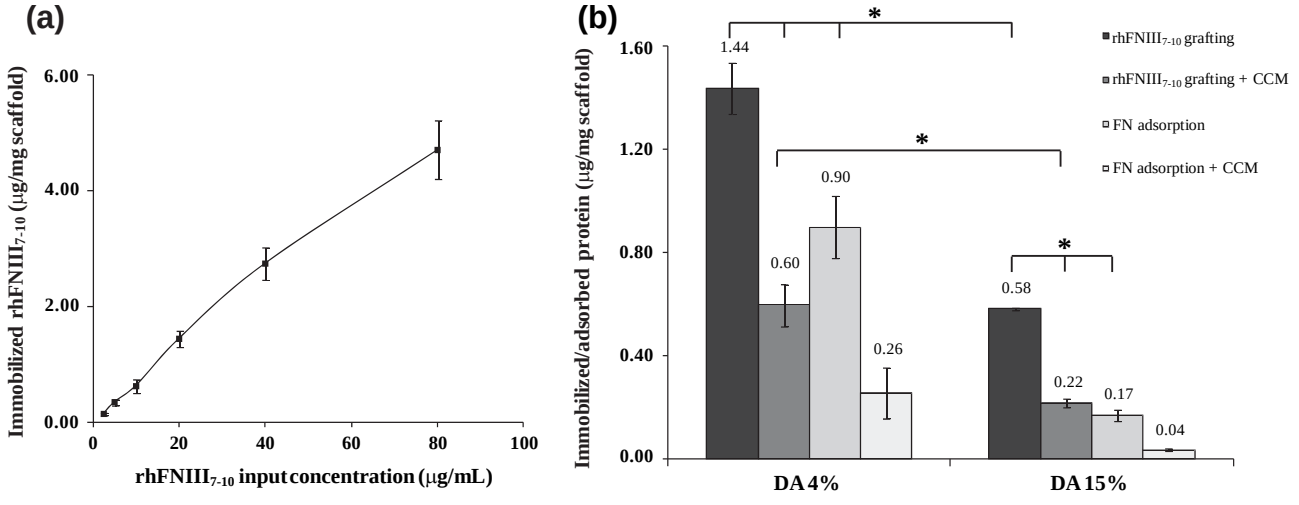

Fig. 4. Quantitation of immobilized $rhFNIII_{7–10}$ on CH porous conduits, as determined using ^{125}I-labelled $rhFNIII_{7–10}$ (mean ± SD; $n = 8$). (a) Immobilized amount of $rhFNIII_{7–10}$ on DA 4% conduits as a function of $rhFNIII_{7–10}$ input concentration. (b) Immobilized amount of $rhFNIII_{7–10}$ on CH porous conduits (DA 4% and 15%) using a 20 $\mu g\ ml^{-1}$ $rhFNIII_{7–10}$ input concentration as well as their retention after further incubation in the serum-containing culture medium used in cell culture assays (CCM) for 24 h. The levels of FN adsorption from a 20 $\mu g\ ml^{-1}$ hFN solution and their retention following incubation in CCM are also shown. * $p < 0.001$.

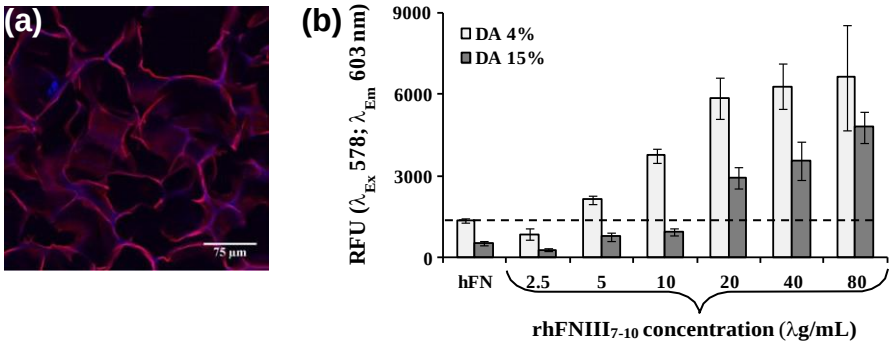

Fig. 5. Distribution and conformation of rhFNIII$_{7–10}$ upon grafting to CH porous conduits (DA 4% and 15%), as probed by immunofluorescent staining of the integrin-binding RGD site of FN in cryosections (in red). (a) CLSM imaging of CH scaffolds (DA 4%) grafted with rhFNIII$_{7–10}$ (20 µg ml^{-1}). (b) Quantitative analysis of exposed cell-binding domains as a function of rhFNIII$_{7–10}$ input concentration, as determined by fluorimetry (mean ± SD; $n = 9$). The dotted line indicates the levels of exposed cell-binding domains provided by incubation of DA 4% scaffolds in a 20 µg ml^{-1} hFN solution.

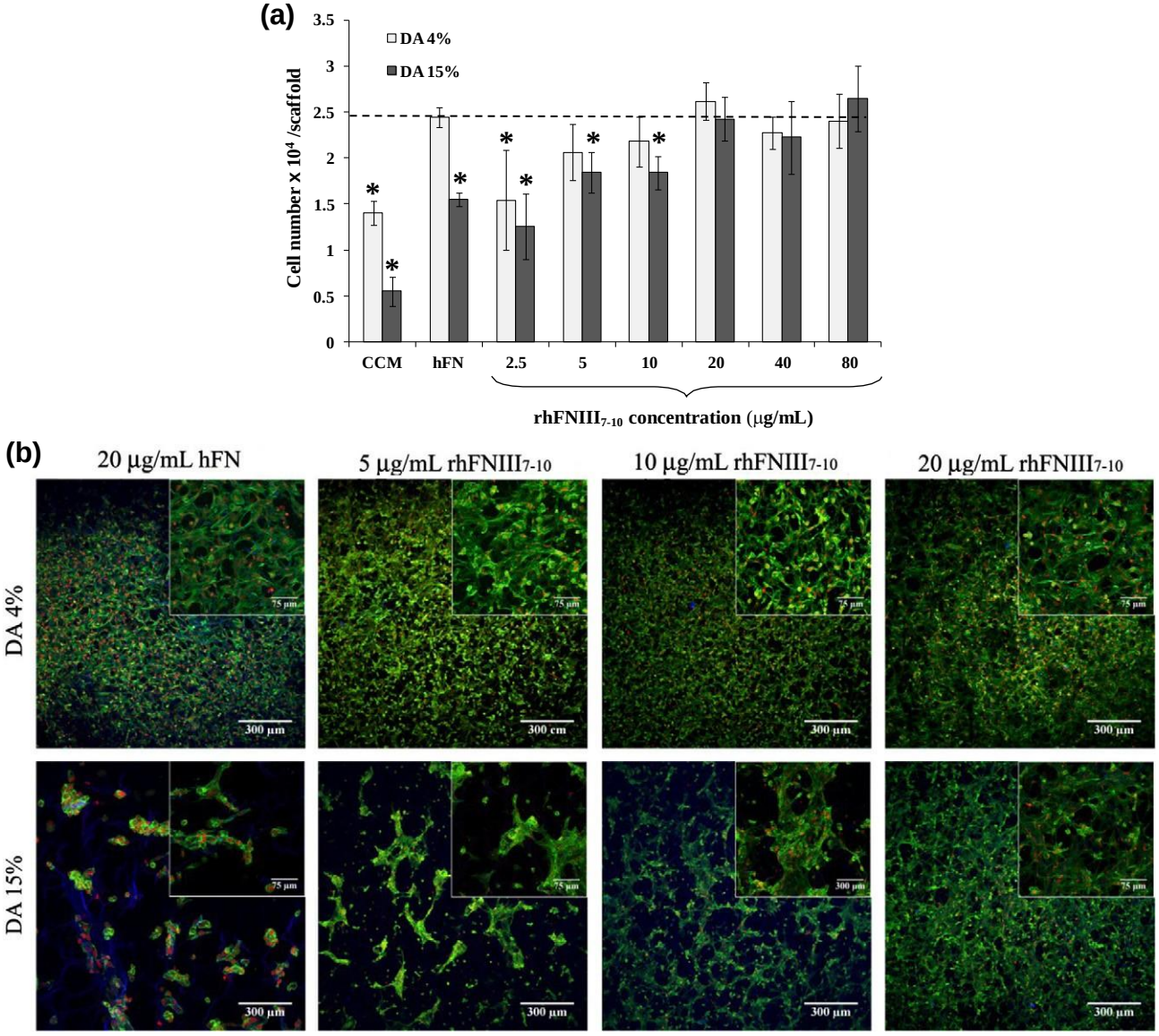

Fig. 6. Cell behaviour of HPMEC-ST1.6R cells on CH porous conduits (DA 4% and DA 15%) grafted with rhFNIII$_{7–10}$. (a) Adhesion of HPMEC-ST1.6R cells as a function of rhFNIII$_{7–10}$ input concentration (mean ± SD; $n = 6$). Results corresponding to CH samples incubated in CCM or in a 20 µg ml^{-1} hFN solution are also shown. * indicates a significant difference (p G 0.05) from cell numbers found on DA 4% scaffolds incubated with hFN (dotted line). (b) Cytoskeleton organization of HPMEC-ST1.6R cells cultured on CH porous conduits grafted with rhFNIII$_{7–10}$ (5, 10 and 20 µg ml^{-1}), as shown by fluorescent labelling of F-actin (green) and DNA (red). Cell cytoskeleton organization on conduits previously incubated in a 20 µg ml^{-1} hFN solution is also shown. Images obtained by CLSM, 24 h after cell seeding. Results show that concentrations of rhFNIII$_{7–10}$ as low as 5 and 20 µg ml^{-1} were sufficient to promote cytoskeletal rearrangement and cell spreading of EC adhered to CH with DA 4% and 15%, respectively.

15% for rhFNIII$_{7–10}$ concentrations ≥20 μg ml^{-1}. Under these grafting conditions (rhFNIII$_{7–10}$ ≥ 20 μg ml^{-1}), cell adhesion on DA 15% was typically 1.4–1.7-fold higher than that provided by passively adsorbed hFN. In accordance with previous results, physiadsorbed hFN was much less effective in mediating EC adhesion to DA 15% compared with DA 4%.

The effect of immobilized rhFNIII$_{7–10}$ on EC cytoskeletal organization was assessed after 24 h of cell culture. In line with fluorimetry and cell adhesion results, F-actin/DNA labelling showed that rhFNIII$_{7–10}$ concentrations of 5 and 20 μg ml^{-1} were sufficient to promote EC cytoskeletal rearrangement on CH with DA 4% and 15%, respectively (Fig. 6b). Under these grafting conditions, a homogeneous distribution of ECs over the inner surface of the porous conduits was achieved on both DAs. Higher magnification CLSM images revealed ECs displaying diffuse F-actin distribution and preferentially oriented along the polymeric pore walls, similarly to those found on DA 4% scaffolds with physiadsorbed hFN (20 μg ml^{-1}, control).

Finally, the angiogenic potential of ECs seeded on the luminal surface of rhFNIII$_{7–10}$-grafted CH porous scaffolds was assessed. For this purpose, a fibrin gel was added to the lumen of the EC-colonized scaffolds and cells cultured for 48 h in the presence of angiogenic inducers. At the end of this time, sprouting of viable ECs from the luminal surface of the scaffolds into the fibrin gel was already visible under CLSM, as well as cell alignment and branching (Fig. 7a). Histology analysis of H&E-stained transversal cryosections also revealed cell migration from the EC-colonized scaffolds into the fibrin gel, as well as the presence of ECs lining lumen-like spaces, suggesting the formation of capillary-like structures (Fig. 7b and c). On DA 4% conduits physiadsorbed with hFN (control), EC behaviour was similar to that described for rhFNIII$_{7–10}$-grafted CH porous conduits (Fig. S8).

4. Discussion

This study aimed to develop a strategy to efficiently promote EC adhesion to CH porous guidance matrices with different DAs. To achieve this goal, covalent binding of a recombinant fragment of human FN (rhFNIII$_{7–10}$) was explored. Although lacking the multiple binding domains present in native hFN for extracellular matrix/growth factor binding and self-assembly, rhFNIII$_{7–10}$ has a smaller size than hFN (42 kDa vs. 440 kDa) [27], while presenting the hFN central cell binding domain with the RGD binding motif and the PHSRN synergy site. As a result, by using rhFNIII$_{7–10}$ one can achieve higher surface densities of cell-binding domains when applying similar amounts of protein. Moreover, owing to the presence of complementary domains and to its spatial conformation, rhFNIII$_{7–10}$ has advantages over short synthetic bioadhesive oligopeptides such as the RGD sequence, by conveying specificity towards α5β1 integrin and leading to higher cell activity both in vitro and in vivo [37,38]. rhFNIII$_{7–10}$ biospecificity towards α5β1 integrin makes it an interesting ligand to mediate EC adhesion, as ECs use predominantly α5β1 integrin to adhere to hFN [39].

The porous conduits developed were tailored to bridge a 4 mm gap in an adult rat complete transection model of SCI (to be used in future in vivo evaluation of the pre-endothelialized scaffolds). Highly porous conduits with porous luminal surface were successfully prepared from CH with DA 4% and 15%, using the moulding system described. For the desired application, a high and interconnected porosity is expected to be beneficial for exchange of nutrients and oxygen with the surrounding tissue. Moreover, the open porosity of the luminal surface was shown to permit infiltration of an EC suspension into the spongy matrix (Fig. 7b and Fig. S8b), despite the smaller size of the interconnection pores. The DA 15% scaffolds showed a significantly higher water uptake compared with DA 4% (also found for CH films), which can be related to the decrease in CH crystallinity [16]. Despite the observed high water uptake, both type of scaffolds retained their original structure following hydration.

It was initially assessed whether passively adsorbed rhFNIII$_{7–10}$ was able to mediate EC adhesion to CH. Results showed that rhFNIII$_{7–10}$ coating concentrations as low as 20 μg ml^{-1} were sufficient to allow EC adhesion and subsequent cytoskeletal organization on DA 4%. However, pre-adsorption of rhFNIII$_{7–10}$ was not able to mediate EC adhesion to DA 15%, regardless of the rhFNIII$_{7–10}$ concentration used. These marked differences in terms of EC behaviour correlated well with the lower amount of adsorbed rhFNIII$_{7–10}$ and lower level of exposed cell-binding domains found on DA 15% compared with DA 4%, following the trend previously observed for the full hFN [20]. It is hypothesized that these differences may be associated with the lower amount of amine groups (with concomitant increase of methyl groups) present on DA 15% compared with DA 4%. Surface chemistry was shown to modulate the amount and the conformation of adsorbed rhFNIII$_{7–10}$, as well as its functional activity [40,41]. In particular, surfaces exposing amine groups were shown to promote rhFNIII$_{7–10}$ adsorption and induce a more favourable conformation of adsorbed rhFNIII$_{7–10}$ for cell adhesion compared with COOH and CH_3 groups, further supporting this assumption [40].

Covalent binding of rhFNIII$_{7–10}$ to CH was then explored using EDC/NHS mediated amidation and 0.1 M MES as solvent. As expected, in the absence of EDC/NHS, minimal amounts of rhFNIII$_{7–10}$ were detected on CH matrices, as shown by immunoflu-

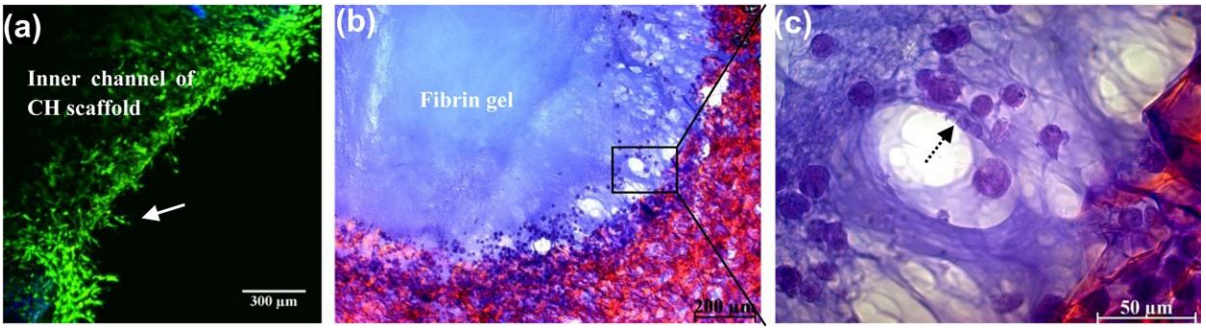

Fig. 7. In vitro angiogenesis potential of HPMEC-ST1.6R cells cultured in CH porous conduits (DA 4%) grafted with rhFNIII$_{7–10}$ (5 μg ml^{-1}). ECs were seeded on the luminal surface of the porous conduits and cultured for 5 days. At this time point, a fibrin gel was added, and cells were cultured for an additional period of 48 h in the presence of VEGF, bFGF and aprotinin. (a) CLSM imaging of hemisectioned conduits previously incubated with Calcein AM/propidium iodide shows sprouting of viable ECs (in green) from CH scaffolds into fibrin. Cell alignment and branching was also observed (solid arrow). Cell migration of ECs into fibrin was also revealed by H&E staining of transversal cryosections (b and c). Dashed arrow indicates EC lining a lumen-like space.

orescent labelling of FN cell-binding domains. Dimethylformamide (DMF) was explored also for EDC/NHS coupling of rhFNIII$_{7–10}$, as this solvent had been used previously by Ho and collaborators [42] for the grafting of RGD sequences to CH porous matrices. However, incubation in DMF resulted in large deposits of aggregated protein (results not shown), possibly due to rhFNIII$_{7–10}$ lower solubility in DMF. Hence DMF was deferred in favour of 0.1 M MES. FTIR results suggest covalent binding of rhFNIII$_{7–10}$ to CH primary amines. Following peptide grafting to CH amine groups, the most evident change expected in the FTIR spectrum of CH is a reduction in the absorbance of the N–H deformation peak in primary amines [42], which was observed.

A linear increase of immobilized rhFNIII$_{7–10}$ with increasing rhFNIII$_{7–10}$ concentration was found, in contrast to the profile of rhFNIII$_{7–10}$ immobilization on two-dimensional surfaces, which usually presents a well-defined saturation plateau [38]. This behaviour is attributed to the high surface area of the porous conduits. Moreover, for the same rhFNIII$_{7–10}$ concentration, higher amounts of immobilized rhFNIII$_{7–10}$ and levels of exposed cell-binding domains were found on DA 4% compared with DA 15%. The higher grafting efficiency observed for DA 4% is possibly related to the larger number of amine groups available for functionalization compared with those present in DA 15%. The immunofluorescence bioactivity assays also showed that, for a specific DA, the levels of exposed cell binding domains on CH can be tuned by varying the rhFNIII$_{7–10}$ concentration in the coupling reaction. Specifically for DA 4% and 15% CH conduits, the lowest rhFNIII$_{7–10}$ concentration required to achieve levels of exposed cell-binding domains similar to or exceeding those provided by passively adsorbed hFN on DA 4% (positive control) was 5 and 20 μg ml^{-1}, respectively. These same rhFNIII$_{7–10}$ concentrations were sufficient to promote EC adhesion and cytoskeletal rearrangement on CH in the range of those observed in the control, in good agreement with the bioactivity levels found. Immobilized rhFNIII$_{7–10}$ was shown, therefore, to be effective in mediating EC adhesion and cytoskeleton organization on CH, which are two key cellular events required for EC proliferation and the establishment of cell–cell contacts, ultimately leading to the formation of a functional EC layer in vivo. A minimum density of hFN cell-binding epitopes is required for integrin clustering, focal adhesion assembly and actin polymerization [43]. Therefore, one may assume that rhFNIII$_{7–10}$ covalent binding was able to provide this minimum density of cell-binding domains to CH with DA 4% and 15%, and that the minimal rhFNIII$_{7–10}$ input concentration is dependent on the DA. Finally, the in vitro angiogenic potential of ECs seeded on rhFNIII$_{7–10}$-functionalized CH conduits was evaluated. Results showed that, besides efficiently mediating EC adhesion and cytoskeletal rearrangement on CH, immobilized rhFNIII$_{7–10}$ does not interfere with EC ability to sprout and form capillary-like structures following the addition of a fibrin gel to the inner lumen of the scaffolds. This EC feature will be essential for the establishment of a functional microvascular network following implantation of the pre-endothelialized conduits in vivo.

In summary, the present results demonstrate that grafting of rhFNIII$_{7–10}$ can be used as a strategy to endothelialize the luminal surface of porous CH conduits with different DAs. To the best of the present authors' knowledge, this is the first report exploring the use of this bioadhesive ligand to promote the endothelialization of porous polymeric structures. This endothelialized conduit is expected to contribute to angiogenesis and to the formation in vivo of a vascular network within the scaffold, which will be beneficial to the survival of the graft following implantation in an SCI. Also, when used as a vehicle for the transplantation of relevant cell types in the context of SCI therapies, pre-endothelialized conduits are expected to contribute to the survival of the transplanted cells. In this manner, endothelialized porous conduits are expected to impact the outcome of cell transplantation therapies in the spinal cord, ultimately leading to long-distance axonal regeneration and improved functional recovery. This hypothesis is currently being investigated by the authors'team.

5. Conclusions

CH porous conduits with porous luminal surface were successfully prepared by TIPS for application in spinal cord regenerative therapies. To promote EC adhesion to CH with different DAs, covalent binding of rhFNIII$_{7–10}$ was explored. The results demonstrate that the amount and levels of exposed cell-binding domains of immobilized rhFNIII$_{7–10}$ can be tuned by varying the rhFNIII$_{7–10}$ concentration in the coupling reaction. Moreover, these parameters were found to be DA-dependent. Finally, it was shown that rhFNIII$_{7–10}$ concentrations as low as 5 and 20 μg ml^{-1} efficiently mediated EC adhesion and cytoskeletal rearrangement on CH with DA 4% and 15%, respectively, without affecting the endothelial angiogenic potential, a fundamental feature for angiogenesis in vivo. Taken together, these results demonstrate that grafting of rhFNIII$_{7–10}$ can be used as a strategy to endothelialize CH porous scaffolds with different DAs, this being of particular interest when matrices with different degradation rates are required.

Acknowledgements

This work was financed by FEDER funds through the Programa Operacional Factores de Competitividade – COMPETE and by Portuguese funds through FCT – Fundação para a Ciência e a Tecnologia in the framework of the Project PEst-C/SAU/LA0002/2011 and PTDC/SAU-BEB/65328/2006).

Appendix A. Figures with essential color discrimination

Certain figures in this article, particularly Figs. 2, 5–7, are difficult to interpret in black and white. The full color images can be found in the on-line version, at http://dx.doi.org/10.1016/j.actbio.2012.10.029.

Appendix B. Supplementary data

Supplementary data associated with this article can be found, in the online version, at http://dx.doi.org/10.1016/j.actbio.2012.10.029.

References

[1] Mautes AEM, Weinzierl MR, Donovan F, Noble LJ. Vascular events after spinal cord injury: contribution to secondary pathogenesis. Phys Ther 2000;80: 673–87.
[2] Barnabe-Heider F, Frisen J. Stem cells for spinal cord repair. Cell Stem Cell 2008;3:16–24.
[3] Thuret S, Moon LDF, Gage FH. Therapeutic interventions after spinal cord injury. Nat Rev Neurosci 2006;7:628–43.
[4] Straley KS, Foo CWP, Heilshorn SC. Biomaterial design strategies for the treatment of spinal cord injuries. J Neurotraum 2010;27:1–19.
[5] Fouad K, Schnell L, Bunge MB, Schwab ME, Liebscher T, Pearse DD. Combining Schwann cell bridges and olfactory-ensheathing glia grafts with chondroitinase promotes locomotor recovery after complete transection of the spinal cord. J Neurosci 2005;25:1169–78.
[6] Tsai EC, Dalton PD, Shoichet MS, Tator CH. Matrix inclusion within synthetic hydrogel guidance channels improves specific supraspinal and local axonal regeneration after complete spinal cord transection. Biomaterials 2006;27: 519–33.
[7] Freier T, Koh HS, Kazazian K, Shoichet MS. Controlling cell adhesion and degradation of chitosan films by N-acetylation. Biomaterials 2005;26:5872–8.
[8] Guerra GD, Barbani N, Gagliardi MC, Rosellini E, Cristallini C. Chitosan-based macromolecular biomaterials for the regeneration of chondroskeletal and nerve tissue. Int J Carbohydr Chem 2011; 2011: Article ID 303708. http://dx.doi.org/10.1155/2011/303708.

[9] Nomura H, Zahir T, Kim H, Katayama Y, Kulbatski I, Morshead CM, et al. Extramedullary chitosan channels promote survival of transplanted neural stem and progenitor cells and create a tissue bridge after complete spinal cord transection. Tissue Eng A 2008;14:649–65.
[10] Zahir T, Nomura H, Guo XD, Kim H, Tator C, Morshead C, et al. Bioengineering neural stem/progenitor cell-coated tubes for spinal cord injury repair. Cell Transplant 2008;17:245–54.
[11] Chen X, Yang Y, Yao J, Lin W, Li Y, Chen Y, et al. Bone marrow stromal cells-loaded chitosan conduits promote repair of complete transection injury in rat spinal cord. J Mater Sci – Mater Med 2011;22:2347–56.
[12] Kean T, Thanou M. Biodegradation, biodistribution and toxicity of chitosan. Adv Drug Deliv Rev 2010;62:3–11.
[13] Mishra OP, Batra P, Ali Z, Anupurba S, Das BK. Cerebrospinal fluid lysozyme level for the diagnosis of tuberculous meningitis in children. J Trop Pediatr 2003;49:13–6.
[14] Zhang KH, Xiao HS, Lu PH, Shi J, Li GD, Wang YT, et al. Differential gene expression after complete spinal cord transection in adult rats: an analysis focused on a subchronic post-injury stage. Neuroscience 2004;128: 375–88.
[15] Varum KM, Holme HK, Izume M, Stokke BT, Smidsrod O. Determination of enzymatic hydrolysis specificity of partially *N*-acetylated chitosans. Biochim Biophys Acta – Gen Subj 1996;1291:5–15.
[16] Tomihata K, Ikada Y. In vitro and in vivo degradation of films of chitin and its deacetylated derivatives. Biomaterials 1997;18:567–75.
[17] Kim H, Tator CH, Shoichet MS. Chitosan implants in the rat spinal cord: biocompatibility and biodegradation. J Biomed Mater Res A 2011;97A: 395–404.
[18] Rak J, Filmus J, Kerbel RS. Reciprocal paracrine interactions between tumour cells and endothelial cells: the 'angiogenesis progression' hypothesis. Eur J Cancer 1996;32A:2438–50.
[19] Kaully T, Kaufman-Francis K, Lesman A, Levenberg S. Vascularization – the conduit to viable engineered tissues. Tissue Eng B Rev 2009;15:159–69.
[20] Amaral IF, Unger RE, Fuchs S, Mendonça AM, Sousa SR, Barbosa MA, et al. Fibronectin-mediated endothelialisation of chitosan porous matrices. Biomaterials 2009;30:5465–75.
[21] Moon JJ, West JL. Vascularization of engineered tissues: approaches to promote angiogenesis in biomaterials. Curr Top Med Chem 2008;8:300–10.
[22] Potts JR, Campbell ID. Structure and function of fibronectin modules. Matrix Biol 1996;15:313–20.
[23] Vachoud L, Zydowicz N, Domard A. Formation and characterisation of a physical chitin gel. Carbohydr Res 1997;302:169–77.
[24] USP harmacopeia 2005 [General chapter 85].
[25] Zhang RY, Ma PX. Poly(alpha-hydroxyl acids) hydroxyapatite porous composites for bone-tissue engineering. I. Preparation and morphology. J Biomed Mater Res 1999;44:446–55.
[26] Aukhil I, Joshi P, Yan Y, Erickson HP. Cell- and heparin-binding domains of the hexabrachion arm identified by tenascin expression proteins. J Biol Chem 1993;268:2542–53.
[27] Hashimoto-Uoshima M, Yan YZ, Schneider G, Aukhil I. The alternatively spliced domains EIIIB and EIIIA of human fibronectin affect cell adhesion and spreading. J Cell Sci 1997;110(Pt. 18):2271–80.
[28] Laemmli UK. Cleavage of structural proteins during assembly of head of bacteriophage-T4. Nature 1970;227:680–5.
[29] Denuziere A, Ferrier D, Damour O, Domard A. Chitosan–chondroitin sulfate and chitosan–hyaluronate polyelectrolyte complexes: biological properties. Biomaterials 1998;19:1275–85.
[30] Amaral IF, Lamghari M, Sousa SR, Sampaio P, Barbosa MA. Rat bone marrow stromal cells osteogenic differentiation and fibronectin adsorption on chitosan membranes: the effect of the degree of acetylation. J Biomed Mater Res A 2005;75A:387–97.
[31] Unger RE, Krump-Konvalinkova V, Peters K, Kirkpatrick CJ. In vitro expression of the endothelial phenotype: comparative study of primary isolated cells and cell lines, including the novel cell line HPMEC-ST1.6R. Microvasc Res 2002;64:384–97.
[32] Amaral IF, Sampaio P, Barbosa MA. Three-dimensional culture of human osteoblastic cells in chitosan sponges: the effect of the degree of acetylation. J Biomed Mater Res A 2006;76A:335–46.
[33] Socrates G. Infrared and raman characteristic group frequencies – tables and charts. 3rd ed. Chichester: Wiley; 2001.
[34] Pearson FG, Marchessault RH, Liang CY. Infrared spectra of crystalline polysaccharides. 5. Chitin. J Polym Sci 1960;43:101–16.
[35] Musale DA, Kumar A. Effects of surface crosslinking on sieving characteristics chitosan/poly(acrylonitrile) composite nanofiltration membranes. Sep Purif Technol 2000;21:27–38.
[36] Keselowsky BG, Collard DM, Garcia AJ. Surface chemistry modulates fibronectin conformation and directs integrin binding and specificity to control cell adhesion. J Biomed Mater Res 2003;66A:247–59.
[37] Petrie TA, Capadona JR, Reyes CD, Garcia AJ. Integrin specificity and enhanced cellular activities associated with surfaces presenting a recombinant fibronectin fragment compared to RGD supports. Biomaterials 2006;27:5459–70.
[38] Petrie TA, Raynor JE, Reyes CD, Burns KL, Collard DM, Garcia AJ. The effect of integrin-specific bioactive coatings on tissue healing and implant osseointegration. Biomaterials 2008;29:2849–57.
[39] Kim S, Bell K, Mousa SA, Varner JA. Regulation of angiogenesis in vivo by ligation of integrin alpha 5 beta 1 with the central cell-binding domain of fibronectin. Am J Pathol 2000;156:1345–62.
[40] Michael KE, Vernekar VN, Keselowsky BG, Meredith JC, Latour RA, Garcia AJ. Adsorption-induced conformational changes in fibronectin due to interactions with well-defined surface chemistries. Langmuir 2003;19:8033–40.
[41] Wang H, He Y, Ratner BD, Jiang SY. Modulating cell adhesion and spreading by control of FnIII(7–10) orientation on charged self-assembled monolayers (SAMs) of alkanethiolates. J Biomed Mater Res A 2006;77A:672–8.
[42] Ho MH, Wang DM, Hsieh HJ, Liu HC, Hsien TY, Lai JY, et al. Preparation and characterization of RGD-immobilized chitosan scaffolds. Biomaterials 2005;26:3197–206.
[43] Coussen F, Choquet D, Sheetz MP, Erickson HP. Trimers of the fibronectin cell adhesion domain localize to actin filament bundles and undergo rearward translocation. J Cell Sci 2002;115:2581–90.